MONITORING METAL COMPLEX CONTAMINANTS IN WATER BY SURFACE-ENHANCED RAMAN SPECTROSCOPY

Stuart Farquharson, Wayne W. Smith, and Yuan-Hsiang Lee
Real-Time Analyzers
East Hartford, CT

ABSTRACT

The Department of Energy is responsible for restoring some 475 billion gallons of contaminated groundwater to environmentally acceptable conditions. However, complete characterization of the groundwater must be performed to select the appropriate remediation strategy (*e.g.* pump and treat, biostimulation, etc.). In the case of heavy metals and radionuclides, which represent 60% of the contaminants, characterization includes chemical identity, concentration, and oxidation state. Through the use of fiber optics and surface-enhancement, Raman spectroscopy appears well suited to performing this subsurface characterization as part of a cone penetrometer system. Spectra provide chemical identification and speciation, surface-enhancement provides detection at part-per-billion concentrations, and fiber optics provide remote sampling. However, current surface-enhanced Raman spectroscopy (SERS) sampling modes, electrodes, colloids, or substrates, are unable to provide quantitative or reversible measurements or both. This paper presents a new SERS material consisting of silver-doped sol-gels capable of quantitative, reversible, and reproducible measurements. SERS of chromate and iron cyanate complexes are given to demonstrate the potential of this new material for subsurface groundwater analysis, along with comparisons to traditional electrolytic SERS.

INTRODUCTION

Prior to today's understanding of the environmental fate of heavy metals and radionuclides, the Department of Energy (DOE) buried these waste materials in various types of landfills throughout the former weapons complex. Unfortunately this practice has led to "475 billion gallons of contaminated groundwater in 5700 distinct plumes..."[1]. Metals and radionuclides represent greater than 60% of the contaminants and pose an imminent threat to surrounding rivers, lakes, and coastal waterways (*e.g.* the Columbia River near DOE's Hanford, WA site)[2]. The DOE is charged with the task of restoring these sites to environmentally acceptable conditions[2]. However, this task is quite complex, requiring a thorough characterization of all contaminants present, as well as their interrelationship with the site hydrology, geology, and biology, before a remediation strategy can be developed (*e.g.* biostimulation for metal uptake)[3,4]. This characterization not only requires identification of the heavy metals and radionuclides present and their relative concentration, but also the oxidation state of the metal[2]. The latter may dictate toxicity and can influence subsurface mobility. For example, Cr^{VI} is carcinogenic, while Cr^{III} is not; $U^{VI}O_2^{2+}$ is soluble in water, while $U^{IV}P_2O_7$ precipitates. In addition to the redox potential, the pH of the subsurface environment can also influence complexation and oxidation state[5,6]. Under acidic conditions CrO_4^{2-} becomes $Cr_2O_7^{2-}$, while some metal complexes are readily oxidized (*e.g.* $Fe^{II} \rightarrow Fe^{III}(CN)_6$). The analysis of DOE groundwater is further complicated by previous practices. As an example, $Na_2NiFe(CN)_6$ was used to precipitate ^{137}Cs in underground storage tanks (UST), such that the supernatant could be drained off and more solid waste added[2]. Sensors that could determine the type, amount, and oxidation state of these metals and radionuclides would allow selecting, as well as assessing remediation strategies[7].

A number of analytical techniques have been employed to identify various chemicals in soils and groundwater[8-15]. This includes mass spectrometry and infrared spectroscopy used to detect halogenated solvents[8,9]; atomic absorption, ion-coupled plasma[10,11], and X-ray fluorescence used to detect trace metals[12,13]; and gamma ray and neutron activation analysis used to detect radionuclides[14,15]. Yet accurate analysis has proven difficult, primarily because the required sample extraction adversely influences the measurements (*e.g.* oxidation, phase separation, and volatilization)[16]. Although several of these techniques have been demonstrated in the field, they remain complex, tedious, and time consuming.

Recently, fiber optic based spectroscopic methods have been used to provide in-situ measurements[17-19]. For example, laser induced fluorescence has been successful at measuring trace BTEX (benzene, toluene, ethylbenzene, and xylenes) in groundwater[20,21], Raman spectroscopy has been successful at monitoring metal ion extraction in environmental clean-up[22] as well as measuring several metal nitrate, nitrite, and cyanate salts from underground storage tanks[23], while surface-enhanced Raman spectroscopy (SERS) measurements have been demonstrated for dense non-aqueous phase liquids in groundwater[24,25]. In fact, SERS may be the most appropriate technique for the analysis of trace contaminants in subsurface plumes. Surface-enhanced Raman spectra provide rich molecular vibrational information allowing chemical identification, it has been used to distinguish oxidation states[26], and recently it has been used to detect single

molecules[27,28]. Finally, both Raman and SERS sample analyses has been performed remote from the instrument through fiber optics[25,29]. This suggests incorporating a SERS based sampling system into a cone penetrometer for subsurface groundwater and UST analysis.

However, an examination of sampling modes presently employed for SERS indicates this approach would be difficult. Since its discovery in 1974[30], three primary methods have been developed that employ metals with the appropriate optical constants and surface feature size to promote the SERS effect and the associated enhancement of Raman scattering by six orders of magnitude or more[31-33]. These methods are: 1) preparation of activated electrodes in electrolytic cells[26,31]; 2) preparation of activated silver and gold colloid reagents[34-36] and; 3) preparation of metal coated substrates[37-39].

Both reversible and reproducible measurements have been performed using electrolytic SERS (ESERS)[40]. However this requires a three-electrode sample cell and an electrolyte of known concentration to perform the necessary oxidation-reduction cycles (ORCs) needed to reactivate the electrode surface with new, uncontaminated sites from one measurement to the next. Colloids are severely limited, in that continuous measurements would require a continuous supply of colloids. Furthermore, pH affects aggregate size and consequently signal intensity, making reproducible measurements unlikely. Substrates appear to have the greatest potential, and designs range from silver evaporated on titania particles[39] to gold sputtered on photolithographically produced glass posts[41]. Most substrates require concentrating the sample on the surface through drying to obtain the largest signal enhancements, in effect making the measurements irreproducible and irreversible. However, successful measurements using flow systems have been obtained with glass posts, but manufacturing costs appear prohibitive.

In an effort to overcome these limitations, we developed metal-doped sol-gels for surface-enhanced Raman spectroscopy. The porous silica network of the sol-gel matrix offers a unique environment for stabilizing SER active metal particles and the high surface area increases the interaction between the analytes and metal particles. The sol-gel can be coated on the end of fiber optics or on the internal walls of a glass flow tube for continuous measurements. We previously demonstrated enhancements of 10^7 by measuring 0.1 nM (1 ng/mL or 300 parts per trillion) *p*-aminobenzoic acid (PABA) in methanol[42,43] and reversibility and reproducibility by measuring PABA in a flow through system. The ability to measure, without influence, the oxidation state of inorganic chemicals are invested in this paper. The results are compared to those obtained using ESERS.

EXPERIMENTAL

All chemicals were spectroscopic grade and purchased from Aldrich (Milwaukee, WI). The sol-gel vials were coated in a manner similar to that previously reported by adding ammonium hydroxide to a solution of silver nitrate, tetramethyl orthosilicate, and methanol[42]. After mixing, 0.2 mL of the sol-gel solution was transferred into a glass vial (2 mL), dried, and heated. The incorporated silver ions were then reduced using dilute sodium borohydride. The vials were washed and dried prior to the addition of a sample solution. The SERS sample vials are commercially available from Real-Time Analyzers (RTA, East Hartford, CT). Electrolytic SERS measurements were performed using a 1 mL volume sample cell constructed of Plexiglas using an in-house design[40]. The silver working electrode, platinum counter electrode, and saturated calomel reference electrode (SCE, Cole Parmer, Vernon Hills, IL) were operated in the transimpedence mode by a potentiostat built in-house. A LabVIEW program was written to control the potentiostat through a data acquisition card (DAQ1200, National Instruments, Austin, TX). It allowed setting potentials and sweep rates, while the amount of charge passed was plotted as a cyclic voltammogram. In general, samples were prepared as 10^{-3}M in 0.1M KCl, and the silver electrode roughened by 3 to 7 ORCs by sweeping the voltage between $-0.2V_{SCE}$ to $+0.2V_{SCE}$ at 50 mV/sec and passing 20 to 50 mcoul per cycle.

All spectra were collected on a prototype Fourier transform Raman spectrometer (RTA)[44]. The system consisted of an Nd:YAG laser (Brimrose) for excitation at 1064 nm, an interferometer built by Online Technologies (OLT, East Hartford, CT) for frequency separation, an uncooled InGaAs detector for signal detection (RTA), and an Intel 400 MHz Pentium II based laptop computer (Dell, Round Rock, TX) for interferometric control, data acquisition (OLT), and analysis (LabVIEW). Additional components included a notch filter (Kaiser, Ann Arbor, MI) and interferometer entrance and exit optics (Edmund Scientific, Barrington, NJ). Fiber optics were used to deliver the excitation beam to the sample and the scattered radiation to the interferometer (one meter lengths of 200 and 365 micron core diameter, respectively, Spectran, Avon, CT). A second notch filter (Kaiser) was used as a beam splitter to direct the excitation beam along the same axis as the collected radiation. A microscope object (20x 0.4 NA, Newport, Irvine, CA) was used to focus the beam into the sample and to collect the scattered radiation back along the same axis. In this co-axial backscattering arrangement, the excitation beam was either passed through the outside glass wall of the SERS sample vials and focused into the silver-doped sol-gel film (0.1 mm thickness) or through a glass window of the electrolytic cell and focused onto the electrode surface. This design allowed spectral acquisition from -950 (anti-Stokes) to 3500 cm^{-1} (Stokes) per scan.

RESULTS AND DISCUSSION

The infrared and normal Raman spectra of $Na_4Fe^{II}(CN)_6 \bullet 10H_2O$ and $K_3Fe^{III}(CN)_6$ were measured and used with literature assignments to assign observed SERS bands and are presented in Figure 1[45,46]. In solution, the anion is an octahedral molecule with a high order of symmetry (O_h), and only a few of the 33 possible vibrational modes are observed[47]. The infrared spectrum of $Na_4Fe^{II}(CN)_6 \bullet 10H_2O$ contains only two bands of relative intensity, the ν_7 Fe-C-N bend (T_{1u}) at 585 cm^{-1} and the ν_6 C-N stretch (T_{1u}) that splits into two bands at 2025 and 2053 cm^{-1} (1632 cm^{-1} is due to coordinated water). There are also only a few bands in the Raman solution spectrum of the Fe^{II} complex, the ν_4 Fe-C stretch (E_g) at 388 cm^{-1} (not shown), and the ν_1 (A_{1g}) and ν_3 (E_g) C-N symmetric stretches at 2058 and 2096 cm^{-1}. In the Fe^{III} complex, the more even distribution of the formal charge presumably results in these modes becoming degenerate, and a single band appears at 2132 cm^{-1}, which is well documented[23].

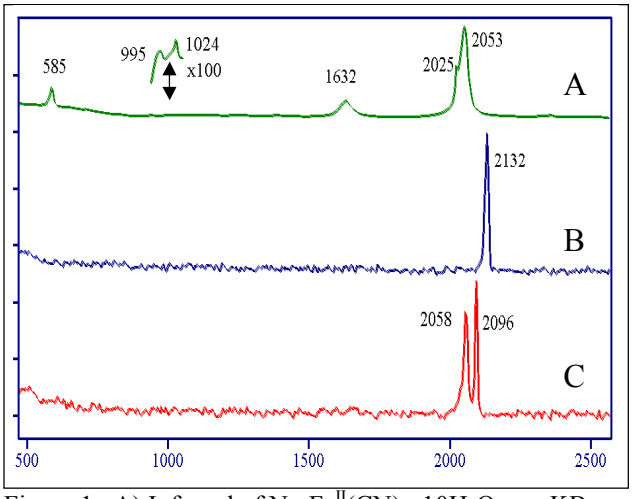

Figure 1. A) Infrared of $Na_4Fe^{II}(CN)_6 \bullet 10H_2O$ as a KBr pellet (1 mg/300 mg KBr), Raman solution spectra of B) 3M $K_3Fe^{III}(CN)_6$ and C) 1M $Na_4Fe^{II}(CN)_6 \bullet 10H_2O$ (S/N=50). Inset: expanded view of IR spectrum. Conditions for B and C: 500 mW of 1064 nm excitation, 8 cm^{-1} resolution, 200 averaged scans, pH of 8 and 4, respectively.

The initial SERS measurements of mM solutions of $Na_4Fe^{II}(CN)_6 \bullet 10H_2O$ and $K_3Fe^{III}(CN)_6$ using the silver-doped sol-gel vials yielded intense spectra that contained a wealth of spectral features (Figure 2). The ν_1 C-N Raman band for the Fe^{II} complex was enhanced by a factor of $1.5x10^5$ in the SER spectrum. This enhancement was based on previously published procedures that ratio normal Raman band intensities, relative sample concentrations, and taking the measurement conditions into account[48]. Most of the new SERS bands can be attributed to the reduction in molecular symmetry due to chemical interactions between the cyanide ligands and silver particles. For example, the ν_7 infrared mode becomes an intense feature at 590 cm^{-1}. This band has been observed by others in ESERS measurements of hexacyanoruthenate complexes[49]. The other two dominant features at 2043 and 2085 cm^{-1} may be attributed to the $\nu_1$and ν_3 C-N symmetric stretches shifted to lower wavenumbers. These peak positions are strongly influenced by the matrix and cation (*e.g.* sodium versus potassium); similar Raman peaks at 2049 and 2072 cm^{-1} have been observed for $Na_4Fe(CN)_6 \bullet 10H_2O$ in the solid phase[23]. In addition, the free CN^- stretch at 2140 cm^{-1} has been reported at 2112 cm^{-1} in ESER spectra[50]. It has been attributed to a tetrahedral $Ag(CN)_3^{2-}$ structure[51]. Alternatively, the 2049 cm^{-1} band could be due to the ν_6 infrared active C-N stretch, while the 2072 cm^{-1} band could represent a surface interaction of one or more of the C-N ligands. In addition to these intense bands, a number of moderately intense bands occur at 507, 520, 680, 920, 995, 1030, and 1157 cm^{-1}, all of which are weakly active in infrared spectra (the broad features between 1200 and 1600 cm^{-1} are considered artifacts). For example, note the 995 and 1024 cm^{-1} bands in the inset of Figure 1. The greater number of spectral features should improve the ability to identify iron cyanide species. Unfortunately, the spectra for the two oxidation states are surprisingly similar. These measurements were discouraging in that the traditional doublet and singlet for the Fe^{II} and Fe^{III} complexes were not observed (Figure 1). Only a shoulder at 2127 cm^{-1} gives an indication that the Fe^{III} complex is present.

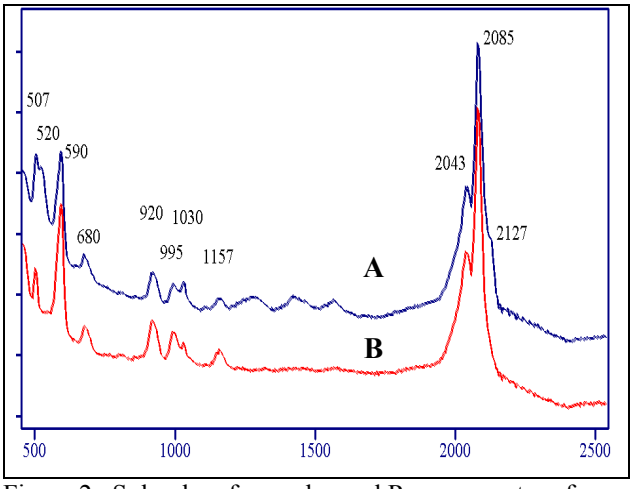

Figure 2. Sol-gel surface-enhanced Raman spectra of A) $3x10^{-3}$M $K_3Fe^{III}(CN)_6$ and B) $2x10^{-3}$M $Na_4Fe^{II}(CN)_6$ (S/N=177). Conditions: 80 mW of 1064 nm excitation, 8 cm^{-1} resolution, 100 averaged scans, pH measured at 6 for both samples.

This prompted a comparison to SER spectra measured at electrode surfaces. Figure 3 shows the ESER spectra of mM $Na_4Fe^{II}(CN)_6 \bullet 10H_2O$ in 0.1M KCl as a function of potential. At -0.1V_{SCE}, the Fe^{II} complex yields a spectrum remarkably similar to its sol-gel SER spectrum, dominated by the bands at 590, 2038, and 2088 cm^{-1}. As the potential of the electrode is driven more negative to -0.9 V_{SCE}, the intensity of the entire spectrum decreases, especially the 590 and 2038 cm^{-1} bands. This is

undoubtedly due to a decrease in interaction between the negatively charged Fe^{II} complex and the electrode, which becomes increasingly negative from -0.1 to -0.9 V_{SCE} as the potential passes through the point of zero charge for silver at -0.65 V_{SCE}. It has been suggested that the virtual disappearance of the 590 cm^{-1} band can be attributed to this decreased interaction and a return to "solution-like" symmetry removing infrared activity in the SER spectrum[49]. The near identical change in intensity of the 2038 cm^{-1} band and the 590 cm^{-1} band as a function of potential, suggests the former is due to the ν_6 infrared active C-N stretch. Unfortunately, the formal potential of the Fe^{II}/Fe^{III}-$(CN)_6$ couple is 0.12 V_{SCE},[5] which is outside the operational potential range of the silver electrode, and a change in oxidation state is not observed. Both oxidation states for hexacyanoiron have been observed on a gold electrode[52]. However, according to the researchers, the two states were not due to a potential dependent, charge-transfer reaction, but due to surface structures stabilized by different supporting electrolyte cations. ESERS has provided fundamental information in elucidating such reactions[26].

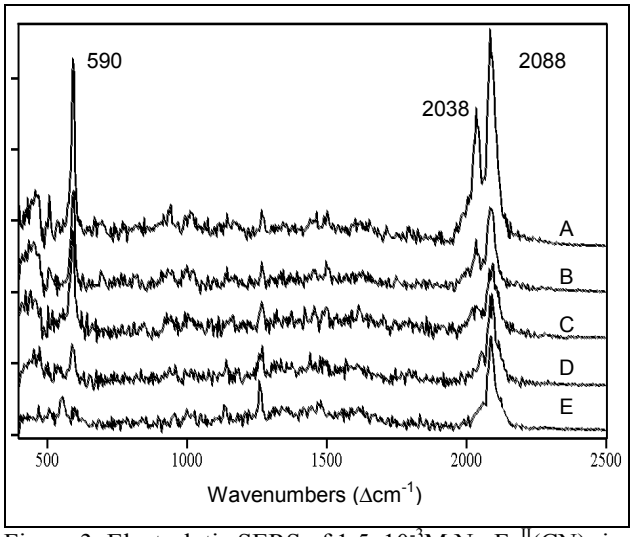

Figure 3. Electrolytic SERS of $1.5x10^{-3}$M $Na_4Fe^{II}(CN)_6$ in 0.1 M KCl at A) -0.1, B) -0.3, C) -0.5, D) -0.7, and E) -0.9 V_{SCE}. Conditions: 200 mW, 200 scans, 8 cm^{-1}.

Figure 4 shows ESERS for $K_3Fe^{III}(CN)_6$, which yielded an enhancement of $1.5x10^4$. The initial spectrum collected at -0.1 V_{SCE} shows even greater similarity to the sol-gel SER spectra containing many spectral features. However, minor infrared bands appear to have greater enhancement than the primary bands at 585 and 2040 cm^{-1}. The Fe^{III} complex ν_1 band observed by others on a gold electrode is absent[52] however. As the potential is made more negative, the spectrum intensity decreases and many modes completely disappear. Interestingly, when the potential is returned to -0.1 V_{SCE}, the spectrum becomes virtually identical to the ESER spectrum obtained for the Fe^{II} complex, and is therefore assigned as such.

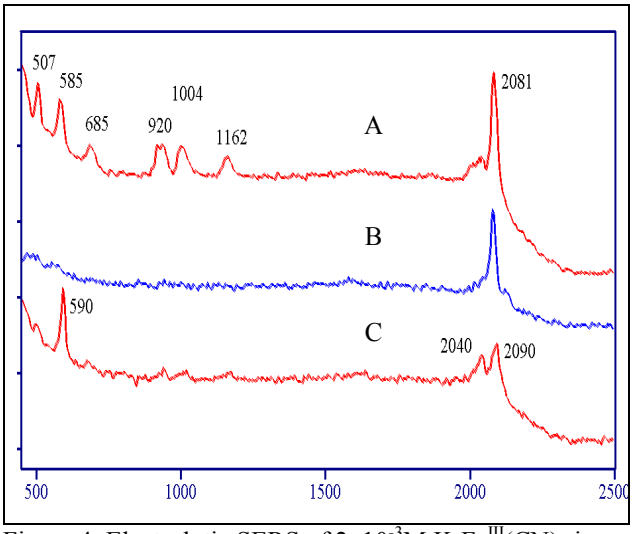

Figure 4. Electrolytic SERS of $2x10^{-3}$M $K_3Fe^{III}(CN)_6$ in 0.1 M KCl at A) -0.1 (S/N=60), B) -0.9, and C) -0.1 V_{SCE} (repeat). Conditions: 200 mW, 100 scans, 8 cm^{-1}.

The SER spectra presented to this point, both electrolytic and sol-gel based, appear to have limited value in analyzing oxidation state of iron complexes in contaminated groundwater. In particular, the ESERS suggests that the Fe^{II} state of the hexacyano complex may preferentially adsorb at silver and dominate the SER spectrum even if the Fe^{III} state is more concentrated in the bulk solution. The sol-gel SER spectra are consistent with this interpretation. However, recent solution phase Raman studies of iron cyanide complexes have shown a marked dependence on pH[23]. Taking this into account, the pH for the two dilute solutions were measured and compared to solutions at near saturation. Not unexpectedly, the pH of the dilute solutions were both near 6, while the 1M solution of $Fe^{II}(CN)_6^{4-}$ was 8 and the 3M solution of $Fe^{III}(CN)_6^{3-}$ was 4. Considering that the pH of contaminated groundwater may cover a wide range, due to various ionic species present (*i.e.* regardless of cyanide concentration), the pH of the iron cyanide solutions were adjusted and the SER spectra re-measured.

Figure 5 shows sol-gel SERS measurements of the dilute Fe^{II} complex adjusted to a pH of 10 using potassium hydroxide, and the dilute Fe^{III} complex adjusted to a pH of 4 using nitric acid. In both cases, the sol-gel coated vials were first thoroughly rinsed with water to remove residual sodium borohydrate (used to reduce the silver). The resultant spectra are distinct and contain bands indicative of their respective oxidation state. At pH 10, the 2042 and 2085 cm^{-1} doublet appears that was previously observed in the ESER spectra for the Fe^{II} complex, while at pH 4 a band at 2131 cm^{-1} appears that corresponds to ν_1 observed in the solution phase Raman spectra of the Fe^{III} complex. In addition, the latter spectrum contains a band at 2090 cm^{-1} and can be assigned to a C-N stretch that involves interaction with the surface of the silver particles. As previously suggested, this surface mode may be re-

sponsible for the 2085 cm^{-1} band observed in the spectra measured at pH 6 and 10, as opposed to the ν_3 assignment.

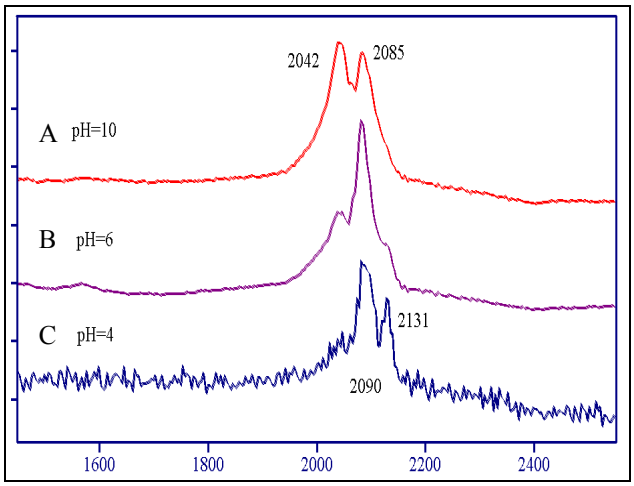

Figure 5. Sol-gel surface-enhanced Raman spectra of A) $Na_4Fe^{II}(CN)_6$ at pH 10, B) $K_3Fe^{III}(CN)_6$ at pH 6, and C) at pH 4. Conditions: 80 mW, 100 scans, but 200 scans for C.

Again, the infrared and Raman spectra of $K_2Cr^{VI}O_4$ were measured to support SER spectral assignments (Figure 6). Since $Cr^{III}_2O_3$ and $Cr^{III}(OH)_3$ are not easily dissolved into solution, are not expected in groundwater, and are non-toxic, only the Cr^{VI} oxidation state was measured. The chromate anion has tetrahedral symmetry in solution (T_d), yielding only four unique spectral modes out of the nine predicted fundamental modes. The infrared spectrum is dominated by the ν_3 asymmetric stretching mode (T_2) at 890 cm^{-1}, with a minor contribution from the ν_1 totally symmetric stretching mode (A_1) at 848 cm^{-1} and the ν_4 bending mode (T_2) at 380 cm^{-1} (not measured). A shoulder also appears at 912 cm^{-1} due to splitting of the ν_3 mode in the solid phase or possibly the presence of the dichromate anion. Conversely, the Raman spectrum is dominated by the ν_1 mode and the ν_2 bending mode (E) at 350 cm^{-1}, with minor contributions from the ν_3 and ν_4 modes. The latter occurs at 375 cm^{-1}. The addition of hydrochloric acid generated the dichromate anion ($Cr_2O_7^{2-}$) both as a precipitate and in solution, as verified by a change from yellow to orange[5]. The Raman spectrum of the precipitate contains additional vibrational modes due to the lower symmetry of the $Cr_2O_7^{2-}$ anion (D_{3d}). The characteristic dichromate bands occur at 235, 364, 375, 388, 912, and 946 cm^{-1}.

The sol-gel SER spectrum of $K_2Cr^{VI}O_4$ yields an intense band at 786 cm^{-1} and a weak band at 596 cm^{-1} (Figure 7). The former band is likely the ν_1 symmetric stretch shifted by interaction with the silver surface. This agrees with previous observations of a similar broad band centered at 796 cm^{-1} reported for the SER spectra of CrO_4^{2-} on silver colloids[53]. It is further supported by the observation that the Raman ν_1 band shifts from 850 to 812 cm^{-1}, when the cation is changed from potassium to silver[54]. Using this assignment, an enhancement of $1.3x10^6$ can be estimated for the SER spectrum based on the normal Raman spectrum. The second band may be due to a weak infrared active chromate band that occurs at 609 cm^{-1} (Figure 6, inset), or complexation with the silver surface. A similar band centered at 610 cm^{-1} has been observed for dichromate at a silver electrode and was assigned to a surface site involving both silver and chromium and symbolized as (AgCr)-O[55].

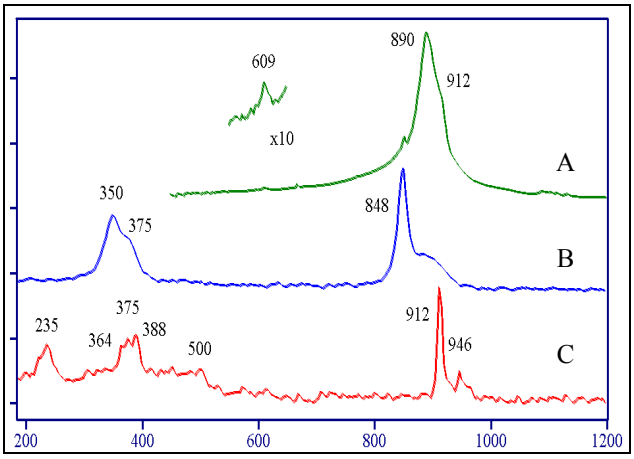

Figure 6. A) Infrared of K_2CrO_4 (KBr pellet), B) Raman of CrO_4^{2-} solution (2M, pH = 8, S/N = 190), and C) Raman of $K_2Cr_2O_7$ as precipitate (pH = 6). Raman conditions: 350 mW of 1064 nm, 200 scans, 8 cm^{-1}. Inset: expanded view of IR spectrum.

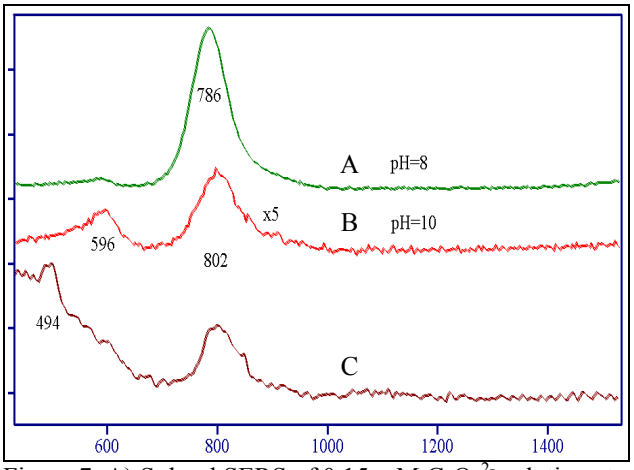

Figure 7. A) Sol-gel SERS of 0.15 mM CrO_4^{2-} solution at pH 8 (S/N = 315), B) at pH 10, and C) ESERS of 1.6 mM CrO_4^{2-} solution (0.1M KCl, -0.1 V_{SCE}, S/N = 33). Sol-gel SERS conditions: 20 mW of 1064 nm, 100 scans, 8 cm^{-1}, ESERS conditions: 50 mW of 1064 nm, 500 scans, 8 cm^{-1}.

Once again, acid and base were added to the dilute chromate solution and the SER spectra were measured. An increase in pH to 10 weakens and shifts the 786 cm^{-1} band to 802 cm^{-1} (as observed on silver colloids), while the 596 cm^{-1} band remains unchanged. This may suggest that the single ligand to silver surface interaction

is weakened, while the (AgCr)-O remains intact. As the solution is made more acidic, the spectrum rapidly disappears, and no spectrum is observed at a pH of 6. It is likely that the combination of chromate and acid, similar to plating processes, passivates the silver through oxidation and deactivates the SERS effect.

The potential dependent ESER spectra for chromate on a silver electrode were also collected. The optimum spectrum was observed at -0.1 V_{SCE} (Figure 7). As the electrode was driven more negative, the primary features at 494 and 802 cm^{-1} simply decreased in intensity. The former band is unassigned. The enhancement for the ESER spectrum was only 10^3, considerably lower than that obtained for the sol-gel SER spectrum (compare S/N and sample conditions in Figure 7). It is, however, worth noting that the ν_1 band at 848 cm^{-1}, although weak, was reproducible.

CONCLUSIONS

Successful SER spectra were obtained using silver-doped sol-gels for $Fe^{II}(CN)_6^{4-}$ and $Cr^{VI}O_4^{2-}$ anions in solution. Enhancement factors were estimated at $1.5x10^5$ and $1.3x10^6$, respectively. These factors appear to be at least an order of magnitude better than enhancement factors obtained by electrolytic SERS. We attribute this to the higher surface area due to the distribution of silver particles throughout the sol-gel, and hence the scattering volume. Detection limits, defined as S/N = 3, can also be estimated based on the measured SER spectra. For a one minute accumulation time (60 scans) and 100 mW of excitation, detection limits are estimated at 1.5 part-per-million ($8.3x10^{-5}$M) and 14 part-per-billion ($8.0x10^{-7}$M) for the two metal anions, respectively. For both complexes, unique vibrational bands were observed that could confidently be assigned with the aid of infrared and Raman spectra, as well as previous studies. The Fe^{II} and Fe^{III} oxidation states of the hexacyanide complexes could be distinguished by bands at 2042 and 2131 cm^{-1}, respectively. It was also found that these bands were strongly dependent on pH, just as the oxidation states are in solution. Also, the enhancement factor for the $Fe^{III}(CN)_6^{3-}$ anion was considerably lower, and detection limits are estimated at 20 ppm. We believe that this preliminary study supports the concept of utilizing SERS to identify metal complexes and their oxidation states in subsurface groundwater. Furthermore, silver-doped sol-gels may be the preferred method of performing these SERS measurements. Measurements can be performed in solution without sample preparation, and the sol-gels can be coated on fiber optic end-faces for incorporation in cone penetrometers.

REFERENCES

1. U.S. Department of Energy Subsurface Contaminants Focus Area (SCFA) at http://www.envnet.org/scfa/ (2001).
2. "Bioremediation of metals and radionuclides...What it is and how it works", A NABIR Primer, web page: www.lbl.gov/NABIR/primer/primer.html (2/2000)
3. O'Brien & Gere Engineers, Inc., *Hazardous Waste Site Remediation: The Engineer's Perspective*, Ed. R. Bellandi, (1988).
4. D.L. Illman, *C&E News*, 9-21, June 21, 1993.
5. D.A. Skoog and D.M. West, *Fundamentals of Analytical Chemistry*, 2nd Ed, Holt, Rinehart and Winston (1969).
6. J.M. Ekert, R.J. Judd, P.A. Lay, and A.K. Symons, *Anal. Chim. Acta*, 255, 31-33 (1991).
7. R.A. Corbitt, *Standard Handbook of Environmental Engineering*, Ch. 9: Hazardous Waste, (McGraw Hill) (1990).
8. M.B. Wise and A.P. Malinauskas, *Characterization, Monitoring and Sensor Technology - Integrated Program: Direct Sampling Ion Trap Mass Spectrometry for Organics in Water, Soil, and Waste*, DOE, NTIS # DE93011563, 11-12 (1993).
9. S.J. Bajic, S. Lou, R.W. Jones, and J.F. McClelland, *Applied Spectroscopy*, 49, 1000-1005 (1995).
10. J. McClelland and J. Corones, *Characterization, Monitoring and Sensor Technology - Integrated Program: Field Deployable VOC analyzer*, DOE, NTIS # DE93011563: 13-14 (1993).
11. R. Lobinski, *Applied Spectroscopy*, 51-7, 260A-278A (1997).
12. D.I. Kaplan, D.B. Hunter, P.M. Bertsch, S. Bajt, and D.C. Adriano, *Environ. Sci. Technol*., 28 (6), 1186-1189 (1994).
13. J.W. Thomason, W. Susetyo, and L.A. Carriera, *Applied Spectroscopy*, 50, 401-408 (1996).
14. J. Tang and C.M. Wai, *Analytical Chemistry*, 58, 3233-3235 (1986).
15. R.L. Brodzinski and P.J. Turner, *Nuclear waste drum assayer*, Pacific Northwest Labs Report SA-17315 (1990).
16. S. Farquharson, P.D. Swaim, P.D., C.P. Christensen, M. McCloud, and H. Friezer, *SPIE*, 1587, 232-239 (1991).
17. A. Ziemba, L. Edwards, B.J. Nielson, *Tunable laser spectrometer and fiber optic site characterization/monitoring solution*, CBD, TYN PRDA 94-0001, Tyndal AF Base, 6/3-9 (1994).

18. K. Kyle, *Conceptual design for a Raman probe for inclusion in the in-tank cone penetrometer*, Lawrence Livermore National Laboratory Report: URCL-ID-I 18962 (1994).
19. J.M.E. Storey, T.E., Barber, R.D. Shelton, E.A. Wachter, K.T. Carron, and Y. Jiang, *Spectroscopy*, 10(3), 20-25 (1995).
20. S. Lieberman, T. Hampton, D. Knowels, M. Davey, and McGinnis, *Comparison of in-situ laser-induced fluorescence (LIF) measurements of petroleum hydrocarbons in soils with conventional laboratory measurements*, Tenth Annual Conference on Contaminated Soils, Amherst, MA (1995).
21. J. Bloch, B. Johnson, N. Newbury, J. Germaine, H. Hemond, and J. Sinfield, *Applied Spectroscopy*, 52, 1299-1304 (1998).
22. R.H. Uibel and J.M. Harris, *Applied Spectroscopy*, 54, 1868-1875 (2000).
23. D.R. Lombardi, C. Wang, B. Sun, A.W. Fountain, T.J. Vickers,C.K. Mann, F.R. Reich, J.G. Douglas, B.A. Crawford, and F.L. Kohlasch, *Applied Spectroscopy*, 48, 875-883 (1994).
24. M.M. Carrabba, R.B. Edmunds, and R.D. Rauh, *Analytical Chemistry*, 59, 2559-2563 (1987).
25. E. Wachter and A.P. Malinauskas, *Characterization, Monitoring and Sensor Technology - Integrated Program: Spectroelectrochemical Sensors for DOE Site Characterization*, DOE, NTIS # DE93011563, 27-28 (1993).
26. S. Farquharson, W.J. Weaver, P.A. Lay, R.H. Magnuson, and H. Taube, *J. Am. Chem. Soc.*, 105, 3350-3351 (1983).
27. K. Kneipp, Y. Wang, R.R. Dasari, and M.S. Feld, *Applied Spectroscopy*, 49, 780-784 (1995).
28. S. Nie and S.R. Emory, *Science*, 275, 1102 (1997).
29. S. Farquharson and S.F. Simpson, *SPIE*, 1796, 272-285 (1992).
30. M. Fleischmann, P.J. Hendra, and A.J. McQuillan, *Chem. Phys. Lett.*, 26, 163-166 (1974).
31. D.L Jeanmaire.and R.P. Van Duyne, *J. Electroanalytical Chem.*, 84, 1-20 (1977).
32. R.L. Gerrel, *Analytical Chemistry*, 61, 401A-411A (1989).
33. K.L. Norrod, L.M. Sudnik, D. Rousell, and K.L. Rowlen, *Applied Spectroscopy*, 51, 994-1001 (1997).
34. P.C. Lee and D. Meisel, *J. Phys. Chem.*, 86, 3391-3395 (1982).
35. J.J. Laserna, A. Berthod, and J.D. Winefordner, *Microchemical J.*, 38, 125 (1988).
36. S.M. Angel, L.F. Katz, D.D. Archibold, L.T. Lin, and D.E. Honigs, *Applied Spectroscopy*, 42, 1327 (1988).
37. Y.-S. Li and Y. Wang, *Applied Spectroscopy*, 46, 142-146 (1992).
38. L. Maya, C.E. Vallet, and Y.H. Lee, *J. Vac. Sci. Technol.*, A 15(2), 238 (1997).
39. T. Vo-Dinh, D.L. Stokes, Y.S. Li, and G.H. Miller, *SPIE,* 1368, 203-209 (1990).
40. S. Farquharson, W.W. Smith, W.H. Nelson, and J.F. Sperry, *SPIE*, 3533-27, 207-214 (1998).
41. J.M.E. Storey, T.E. Barber, R.D. Shelton, E.A. Wachter, K.T. Carron, and Y. Jiang, *Spectroscopy*, 10, 20-25 (1995).
42. Y.H. Lee, W. Smith, S. Farquharson, H.C. Kwon, M.R. Shahriari, and P.M. Rainey, *SPIE*, 3537, 252-260 (1998).
43. Y.-H. Lee, S. Farquharson, and P.M. Rainey, *SPIE*, 3857, 76-84 (1999).
44. S. Farquharson, W. Smith, R.C. Carangelo, and C. Brouillette, *SPIE*, 3859, 14-23 (1999).
45. K. Nakamoto, *Infrared Spectra of Inorganic and Coordination Compounds*, 2nd Ed., (John Wiley & Sons) 1970.
46. R.A. Nyquist, C.L. Putzig, and M.A. Luegers, *Infrared and Raman Spectral Atlas of Inorganic Compounds and Organic Salts*, V2 and V4, (Acad. Press) 1997.
47. W.T. Griffith and G.T. Turner, *J. Chem. Soc., A*., 858-862 (1970).
48. M.J. Weaver, S. Farquharson, and M.A. Tadayyoni, *J. Chem. Phys.*, 82, 4867-4874 (1985).
49. C.G. Allen and R.P. Van Duyne, *JACS*, 103, 7497-7501 (1981).
50. R. Dornhaus, M.B. Long, R.E. Benner, and R. Chang, *Surf. Sci.*, 93, 240 (1980).
51. R.E. Benner, R. Dornhaus, R. Chang, and B.L. Laube, *Surface Science*, 101, 341 (1980).
52. M.D. Fleischmann, D. Sockalingum, and M.M. Musiani, *Spectrochemica Acta*, 46A, 285-294 (1990).
53. H. Feilchenfeld and O. Siiman, *J. Phys., Chem.*, 90, 2163-2168 (1986).
54. R.L Carter, C.E. Bricker, *Spectrochemica Acta*, Part A, 27, 569 (1971).
55. P.B. Dorain and J. L. Bates, *Langmuir*, 4, 1269-1273 (1988).